

Towards 3D printing with tailored local chemical composition by integrated multi-material Additive Manufacturing

Boseila, Jonas^{‡,1}, Rommerskirchen, Max^{‡,1}, Bold, Sebastian¹, Schleifenbaum, Johannes Henrich¹

RWTH Aachen University, Digital Additive Production (DAP), Aachen, Germany

‡ These authors contributed equally

https://doi.org/10.58134/fh-aachen-rte_2022_002

Abstract

A new machine concept combining the Laser Powder Bed Fusion (LPBF) process with a dispensing system to create three-dimensional multi-material AM parts has been developed. Here, we report the combination of stainless-steel parts with locally applied copper coatings using a drop-on-demand (DoD) and continuous material deposition of a copper paste. The influence of the process parameters for the deposition, subsequent drying and fusion of the Cu on the film properties was studied. While the combination of Cu structures with stainless steel from LPBF was achieved, further development is still necessary to achieve defect-free films of pure copper as damage to the film occurred during drying and remelting. This work is a first step towards three-dimensional, multi-material parts with discrete, horizontal and vertical interfaces that are manufactured using a single, integrated machine.

Zusammenfassung

Es wurde ein neues Anlagenkonzept entwickelt, das den Laser Powder Bed Fusion (LPBF)-Prozess mit einem Dosiersystem kombiniert, um dreidimensionale Multimaterial-AM-Teile herzustellen. Hier berichten wir über die Kombination von Edelstahlteilen mit lokal aufgetragenen Kupferschichten unter Verwendung eines Drop-on-Demand- (DoD) und eines kontinuierlichen Materialauftrags einer Kupferpaste. Der Einfluss der Prozessparameter für die Abscheidung, die anschließende Trocknung und das Aufschmelzen des Cu auf die Schichteigenschaften wurde untersucht. Während die Kombination von Cu-Strukturen mit rostfreiem Stahl aus LPBF erreicht wurde, sind noch weitere Entwicklungen notwendig, um defektfreie Schichten aus reinem Kupfer zu erreichen, da beim Trocknen und Umschmelzen Schäden an der Schicht auftraten. Diese Arbeit ist ein erster Schritt auf dem Weg zu dreidimensionalen, multimaterialen Teilen mit diskreten, horizontalen und vertikalen Schnittstellen, die mit einer einzigen, integrierten Anlage hergestellt werden können.

1. Introduction

In the past few years, Additive Manufacturing (AM) technologies have gained interest as a means to manufacture highly complex three-dimensional parts by using either metallic, polymeric, ceramic or composite materials [1–3]. Current applications of these AM parts are moving rapidly to the fabrication of functional components, leading to increasing requirements for these parts in terms of functionality, level of integration, and manufacturing costs [4,5]. To meet the economic and technological challenges of the coming decades, future manufacturing processes must not only be able to flexibly cover the required wealth of variants, but also include direct integration of mechanical or electrical technology components in the produced parts [6]. A promising approach meeting the requirements and at the same time the high demand is the use of different AM technologies. However, to exploit AM's full potential in this regard, the development and processing of new materials and material combinations in the field of multi-material AM will be necessary. One relatively new and promising approach is the implementation of a multi-material machine combining Laser Powder Bed Fusion (LPBF) technology with a dispensing system to enable control over the local chemical composition. One material is provided by the metal powder bed of the LPBF process, while a different material can be applied locally using a drop-on-demand (DoD) approach as well as a continuous material deposition approach using the dispenser.

Using a dispensing system in additive manufacturing is already established in the field of printed electronics, integrated heat structures or for the functionalization of surfaces [7]. With this technology a paste-like material is applied on a substrate and subsequently dried. This production technology is an outstanding solution for the manufacturing of sensors, transistors diodes but also for the local adaptation of coatings. It is already possible to print different types of sensors to measure values such as temperature, pressure, humidity or mechanical load [8].

A significant advantage of the multi-material concept is the introduction of an additional dimension: On top of the high freedom in the three spatial dimensions, the dimension of chemical composition at each point in space is added. This further dimension can be exploited to tailor the local properties of the parts to optimize properties such as corrosion resistance, thermal resistance and conductivity, electrical conductivity, surface properties and catalytic activity.

Furthermore, the life cycle of metal parts can be extended by the implementation of a multi-material concept and the consideration of position-dependent requirements. These include components for the aerospace industry, such as an igniter for a satellite engine, which must be heat-resistant, but also contain conductive areas [9]. Components which improve heat flows via specifically introduced paths made of thermally conductive material, or the integration of electronic components in a single, digitally controlled manufacturing step, are just a few possible future example applications.

In this paper, we focus on the feasibility to build three-dimensional, multi-material parts by combining these two technologies in one hybrid machine, which has been developed by DAP Aachen, Aconity3D and Optomec. The experiments include the investigation of the application of a copper paste by means of a dispensing system to stainless-steel LPBF manufactured components.

Keywords: Integrated Additive Manufacturing, Multi-material, Dispenser, Printed Electronics, Integration of Functions

2. Methods and experimental situation

In this chapter a new machine concept to manufacture multi-material AM parts is presented. The machine is based on an industrial LPBF machine from Aconity3D and additionally equipped with a unit from Optomec, which contains an aerosol jet printing system as well as a dispensing system to apply a second material on 3D-printed surfaces. In this paper, the combination of the LPBF process with the dispensing system is used. A schematic representation of the developed hybrid machine is shown in fig. 1. The two functional principles and the associated challenges resulting from the combination of the two technologies are presented below.

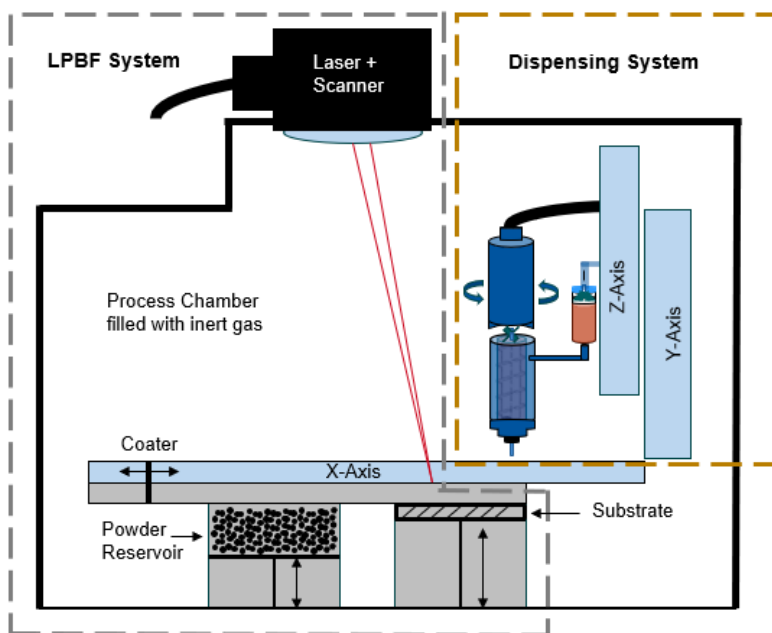


Figure 1: Schematic Representation of the multi-material machine combining the LPBF process with a dispensing system

In the LPBF process, a laser beam as an energy source melts and fuses metal powder according to a given path on each layer. The powder is supplied and the thickness is adjusted by means of two movable cylinders. The process continues layer by layer until the products are completely built. Based on the material properties, the machine settings as well as the process parameters may change to achieve the best quality of the products [10,11].

The dispensing system as a direct writing technology is used to deposit a second material in form of a paste with a dynamic viscosity in a range between 50 and 70.000 mPa·s through screw-type extrusion [12,13]. A schematic representation of the functional principle is shown in figure 2. The operating principle is based on a spiral-shaped spindle that takes up a defined quantity of material and conveys it continuously along a cylinder. The material is fed into the system via cartridges.

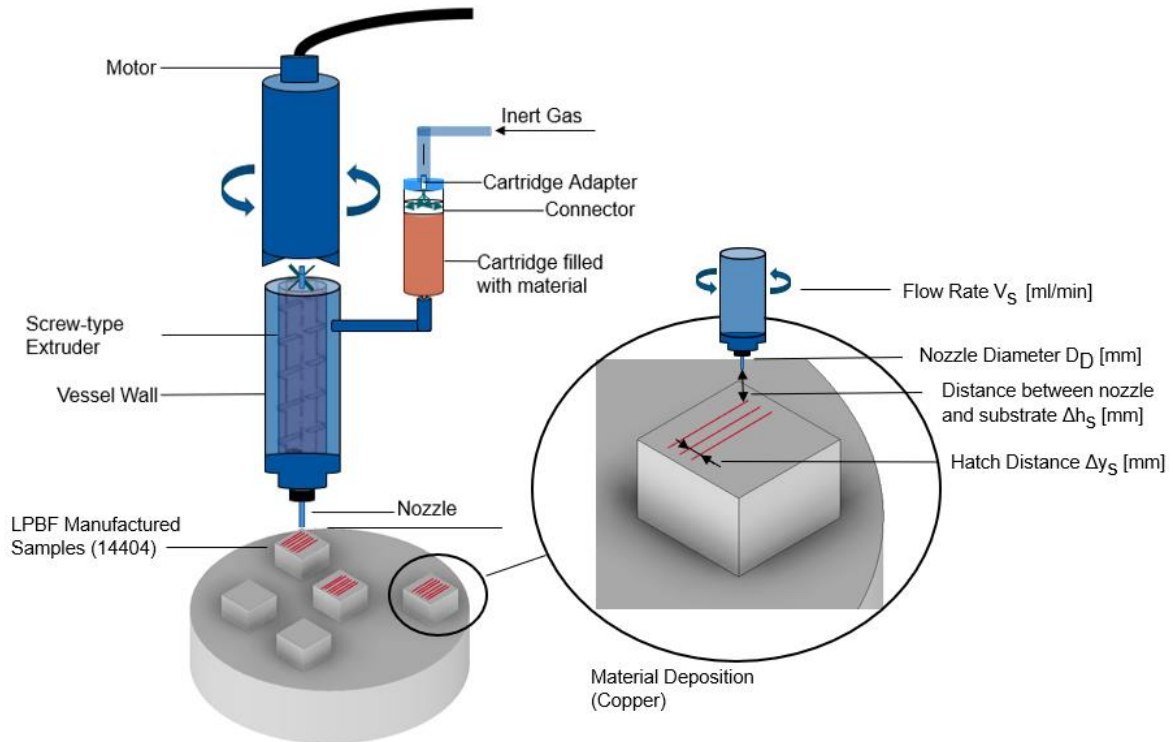


Figure 2: Schematic representation of the functional principle of the dispensing system

The deposition of the material can be done with a continuous or a DoD approach. The latter is characterized by its high accuracy and the possibility to prevent dripping of the nozzle by moving the screw-type extruder in the opposite direction between depositions [14–16].

The continuous extrusion approach maximizes the build rate when using the dispenser, up to a deposition rate of $3.3 \text{ mL}\cdot\text{min}^{-1}$. With regard to the material, certain viscoelastic and rheological properties must be determined so that the material can be deposited smoothly by the deposition head. In particular, a shear-thinning rheological behavior, which is characterized by decreasing viscosity with increasing shear rate, is required for optimal application of the structures [17,18]. A post-treatment in form of drying, heating or sintering is necessary after the deposition to cure the printed structures and improve their mechanical properties. This thermal treatment leads to the removal of solvents and other additives present in the paste in order to enable coalescence of the particles afterwards. To obtain printed structures with the desired properties, a multitude of parameters need to be controlled, among them the energy input of the laser, the nozzle size, the speed of the dispenser, the track pitch and the distance between the nozzle and the substrate [19,18].

3. Results and discussion

3.1. Characterization of the dispenser system

With the objective of producing homogeneously defined and dense structures of dry nanoparticles without solvents, stabilizers or additives, the characterization of the dispenser system was carried out in several steps. As with other nozzle-based processes, the minimum and maximum feature sizes are a function of the nozzle diameter [20]. The nozzle diameter was selected to be comparatively large (0.8 mm) in order to minimize the process uncertainties that can occur due to nozzle clogging, even

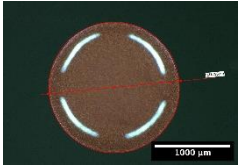
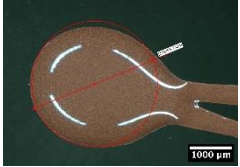
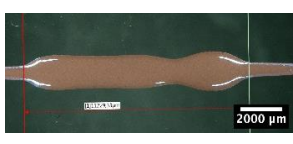
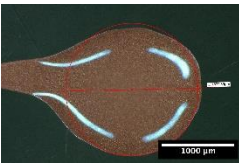
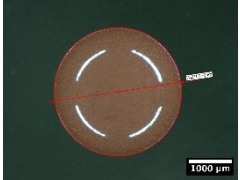
with a nozzle that is 1000 times larger than the nanoparticles used [21]. On the one hand, this is necessary to define to which extent the chemical composition can be tailored locally. This includes the width, height, and length of a single track for modelling a continuous approach of material deposition, as well as the diameter and height of a punctual material deposition with respect to the modelling of a drop-on-demand approach. On the other hand, the predefined material application is crucial to accurately represent the desired discrete or continuous interfaces and to calculate the required amount of material in advance by considering the desired composition. In a first step, the system-relevant process parameters, shown in Fig. 2, were varied for this purpose. The qualitative influence of the respective process parameters on the structural characteristics are summarized in the appendix, Table A1.

Furthermore, the determination of the applied material quantity and the comparison with the calculated target material quantity based on the used volume flow is of special interest. A qualitative study of the dependence of the ratio of actual to target material quantity on the volume flow rate was performed by adjusting the viscosity of the paste by adding ethanol. With an increase in viscosity, a decrease in the actual to target ratio was observed. For very highly viscous media, a ratio of 50 % can be observed in the most favorable case. In order to compensate for the decreasing material discharge, an inlet pressure must be applied to the medium in the case of a highly viscous medium. The lowest standard deviation in the deposited material quantity, i.e. the most precisely controllable deposition, was achieved at a volume flow of $0.2 \text{ mL}\cdot\text{min}^{-1}$ and an inlet pressure of 8 bar.

In a second step, during the material application of individual tracks and dots, essential process parameters and interactions were identified, which significantly influence the morphology of the deposited structures. The critical parameters, in addition to those previously mentioned, include the substrate distance Δh_s and the speed of the dispenser or dwell time, respectively. The results for these variations are shown in Table 1.

For a larger substrate distance, the adhesive force to the substrate is lower than for a smaller one. Thus, the adhesive force to the nozzle must be compensated by the gravitational force acting on the medium, which correlates positively with the dispensed amount of material. In turn, the gravitational force correlates negatively with the dispenser speed for continuous material deposition and positively with the dwell time for spot application. Accordingly, in the case of a large Δh_s of 0.5 mm, the copper structures become more homogeneous as the holding time increases and the dispenser speed decreases. At a low Δh_s of 0.1 mm, the adhesive forces between substrate and medium are dominant irrespective of the studied process parameters. If the holding time increases or the dispenser speed decreases in such a scenario, the adhesive force between substrate and medium and the gravity force dominate. In consequence, at higher speeds, homogeneous structures can initially be deposited before the adhesive force and gravity force together cause excess material to be slightly dragged along in the dispenser direction, thus affecting the morphology of the copper structures. As an example, Table 1 shows the structure characteristics for single tracks and single dots deposited at different Δh_s as well as dispenser speeds and holding times, respectively.

Table 1: Structure characteristics for single tracks and single dots deposited at different Δh_s as well as dispenser speeds and holding times

Substrate distance	Continuous approach of material deposition at different dispenser speeds		DoD approach of material deposition at different holding times	
	$200 \text{ mm}\cdot\text{min}^{-1}$	$800 \text{ mm}\cdot\text{min}^{-1}$	1 s	5 s
0.1				
0.5				

3.2. Process development of the laser exposure

3.2.1. Drying step

In order to achieve homogeneously defined and dense structures consisting of dry nanoparticles without solvents, stabilizers or additives, it is necessary to first dry the deposited films by a laser exposure which can then be followed by a second, more intense exposure that melts the deposited nanoparticles and fuses them together. To produce high-quality films, the influence of the laser exposure during the drying step on the film quality by variation of laser power, laser defocusing and scanning speed was studied. The dryness of the applied structures was controlled qualitatively using a mechanical separation from the substrate with a knife tip. An example of this process for a) a wet and b) a dry specimen is illustrated in the appendix Fig. A1.

Additionally, material loss during exposure was quantified by measuring the weight of the applied structure before and after exposure. Ideally, the mass difference between the two measurements corresponds to the mass of solvent and additives contained in the paste. A mass difference in excess of this amount is caused by a loss of metal particles which is detrimental for the manufacture of a dense, continuous interface with a specific composition in different areas. Based on the specific heat capacity and enthalpies of evaporation of the respective components of the copper paste, a necessary line energy to completely evaporate the additives and solvents was calculated and initially considered as a reference value regarding the laser exposure. The calculated values are stated in the appendix, Table A2, as well as the calculation method (Equations 1-5).

Furthermore, it must be considered that different materials possess different absorption coefficients for radiation of a given wavelength which must therefore also be included in the necessary total line energy. Due to the absence of an absorption band at 1064 nm – the central wavelength the laser used in the machine – for the solvents and additives in the paste, the absorptivity of the paste was assumed

to be identical to that of pure copper at this wavelength, namely 1.4 %. [22]. Likewise, the previously determined ratio of actual to target material discharge must be factored in. For 3-methoxy-3-methyl-1-butanol, a total line energy of $0.430 \text{ J} \cdot \text{mm}^{-1}$ can be calculated, and for the glycolic acid, $0.152 \text{ J} \cdot \text{mm}^{-1}$. Evaporation was performed at maximum defocus of the laser, with a focus diameter of 0.87 mm, to reduce the number of scan vectors per exposed track and thereby minimizing the influence on the morphology of the structures as much as possible.

A single exposure (120 W and $15,000 \text{ mm} \cdot \text{s}^{-1}$) of the copper structures, which were applied by using a small nozzle of 0.5 mm, lead to the evaporation of the solvents and the application of homogeneously defined and dry copper structures. If the material amount is raised by either increasing the volume flow or the nozzle size, not even multiple exposure of the applied structure caused the structures to dry out and be freed from the additives. The maximum possible laser power of 400 W combined with high scan speeds resulted in a strong impact on the deposited copper structures during the process of solvent evaporation. Burning, sintered particles and delamination of copper elements were observed on the substrate surface. The same phenomena were observed with the combination of the minimum power of 1 W and high travel speeds, which should minimize the energy input on the films. Due to the fact that the evaporation is carried out in an oxygen-rich atmosphere without inert gas, the combination of low traveling speeds with high laser powers, i.e. a high energy input, was neglected. This is object of further studies. The material loss, determined by weighing the structures before and after the exposure, varied greatly in a range of approximately 10-30 % for the 0.8 mm nozzle and between approximately 10-60 % for copper structures applied via the 0.5 mm nozzle. The measured material loss results confirm that not only solvents are lost during evaporation as the solvents only account for a mass fraction of 12 % of the paste. The fact that the material loss is greater even for structures that are not completely dried underlines even further that a loss of copper is responsible for the large material loss.

Underlying the analysis of the influence of laser power and scan speed during the drying step on the film quality are the energy and mass transfer processes occurring during and after exposure: Initially, Cu particles in the paste absorb the incoming radiation, raising their temperature. Due to the exponentially falling radiation intensity inside the deposited film, the top layers of Cu particles absorb the majority of absorbed photons. The resulting temperature difference between the particles of the top layer and a) the surrounding solvent and b) the lower parts of the film that experience a lower radiation intensity lead to heat transfer from the Cu particles at the film surface to the rest of the film. Due to the short interaction time between the laser and the deposited film, there is not enough time during the film exposure for diffusion processes of solvent molecules from the lower layers of the film to the surface to occur. While the time-resolved heat transfer and diffusion processes during and after exposure certainly merit a detailed study using, for example, simulative methods, a rough approximation shows we can assume the premise of laser exposure and solvent diffusion occurring on completely different timescales: while the exposure times in the parameter space studied lie in the range of ca. 50-500 μs , the time for solvent molecule diffusion from the substrate-film interface to the film surface is about 5 s at room temperature (using the diffusion coefficient for glycolic acid in water at 25°C [23] and a film thickness of 100 μm). Therefore, the exposure time is close to 10^5 times shorter than the time needed for diffusion and the latter can therefore be neglected during the timescale of exposure. As a result, the solvents undergo a sudden, explosive evaporation inside the copper track when heated above their boiling point. The volume expansion associated with the evaporation leads to damage to the copper film as drops of paste or chips of already dried structures are carried away by

the expanding gas.

Ultimately, the drying out of the structure could be explained by a delayed heat transfer from the heated copper particles on the surface to the rest of the film by heat conduction and convection towards the lower layers. This slower process could then give enough time for the solvent molecules to diffuse to the surface of the film and evaporate there.

These experiments show that not only the total amount of energy introduced into the film matters, but that the timescale during which this occurs is crucial for a complete and homogeneous drying without damage to the film. Here, further work is needed to achieve this goal.

3.2.2. Fusion step

Following the parameter study for the drying of the applied copper paste, the necessary exposure parameters for the fusion of the dry structures with the austenitic chromium-nickel steel base material (316L) was investigated, as well as the possible combinations with the LPBF process. The sample geometry used for the multi-material structure consisted of four copper dots applied by means of DoD in the four corners of the base surface and ten meander-shaped copper tracks in the center of the base surface. (Fig. 3)

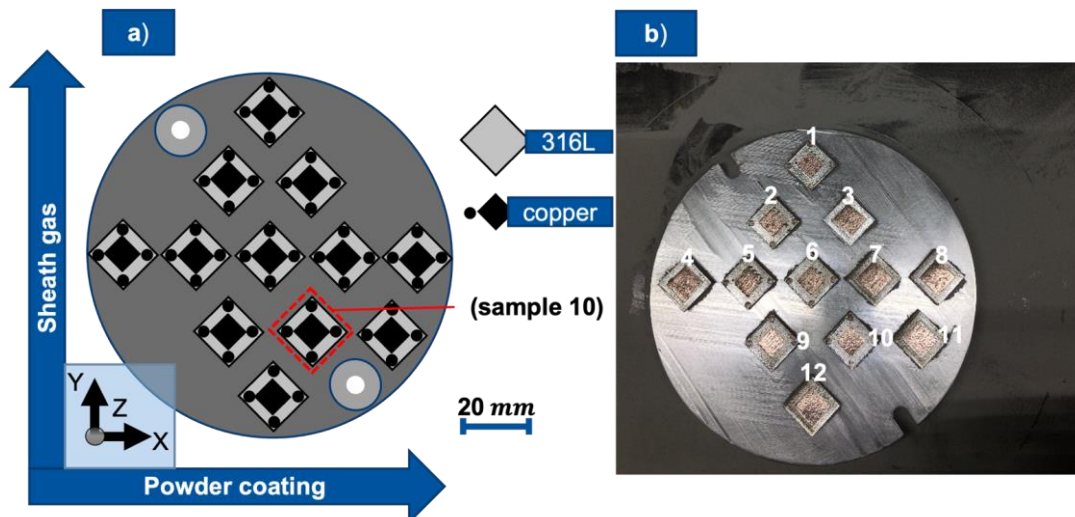


Figure 3: Combined steel-copper parts obtained by LPBF and dispenser. Left: Schematic orientation of the specimens on the substrate plate including sheath gas and powder coating direction of the LPBF process. Right: Image of the construction chamber with constructed samples.

In order to produce homogeneously defined, dense and defect-free horizontal as well as vertical interfaces by combining different printing techniques, the identification and qualification of influencing variables is crucial. As before, the copper structures were exposed starting from the calculated line energy at maximum defocus. For copper, the total line energy for fusion is $32.257 \text{ J} \cdot \text{mm}^{-1}$. Due to insufficient energy input when using this line energy in the experiment, the copper films were not fully melted and were partly lost during the subsequent sample separation.

Accordingly, a parameter variation at higher intensities was performed. The focal diameter was not changed between the standard LPBF process and the exposure of the copper structures and was $80 \mu\text{m}$. The process parameters were evaluated by measuring the density of the respective copper-rich areas and comparing them with the density of the base material. The best results were obtained with a laser power of 250 W and a scan speed of $1,666 \text{ mm} \cdot \text{s}^{-1}$, resulting in a relative density of 98.76% for

the copper-rich areas (Table 2). At lower laser power, the copper is insufficiently fused, resulting in higher porosity. In contrast, at higher powers than 300 W, barely any copper can be detected. Possible causes could be a) the dominant dynamic effects in the laser-material interaction, so that more and more copper is scattered away from the substrate, or b) possible evaporation of the copper due to the high energy input.

Table 2: Comparison of the relative density of the copper tracks for different exposure parameters during the fusion step

Laser power / W	Scan speed / mm·s ⁻¹	Relative density / %
150	1000	97.99
200	1333	98.25
250	1666	98.76
300	2000	98.08

A further point of interest is the optimum order when working with both LPBF and the dispenser in a combined process: whether to apply the dispensed paste before or after melting the powder bed material in the LPBF process in each layer and whether to apply the fresh powder layer before or after exposing the copper paste. The latter variation is important for cases where the structure made of the paste material is embedded in the LPBF part. This means that after application of the paste-based structure, the LPBF process is continued and further layers of metal powder must be distributed. All four possible variations were studied and the results are summarized in Figure 4.

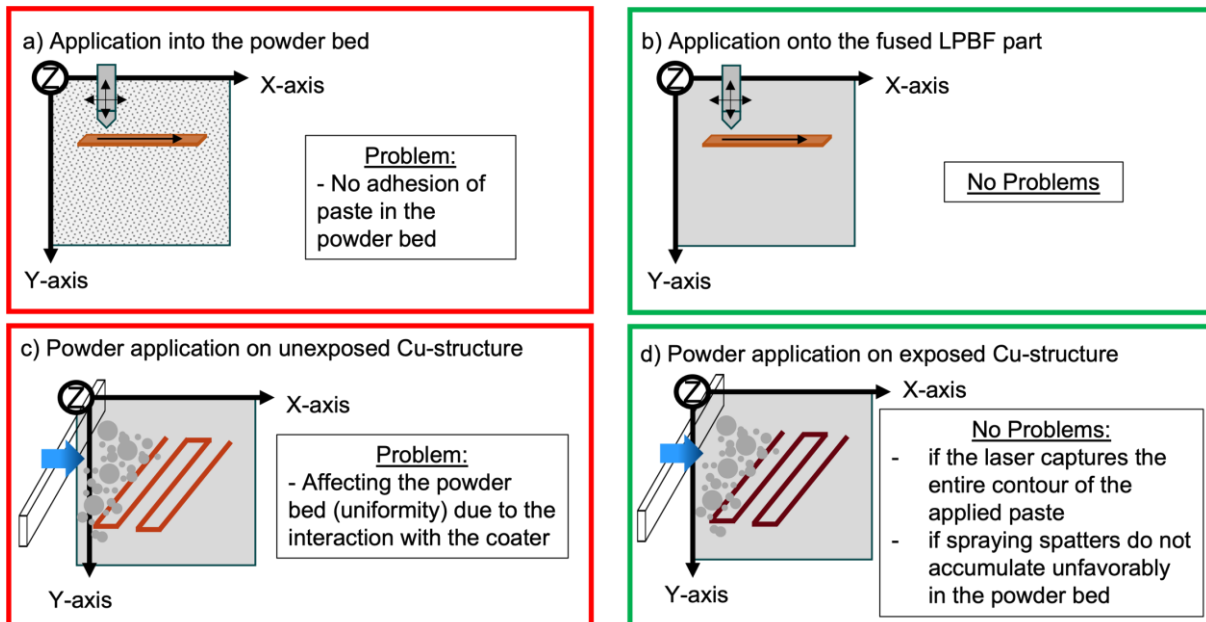


Figure 4: Illustration of the possible orders for material application

During application of the Cu paste directly into the powder bed metal powder stuck to the copper paste while the latter was dragged along by the dispenser, leading to a deviation in geometry from the

CAD file (Fig. A2 in the appendix). This behavior is due to insufficient adhesive force between metal particles in the powder bed that cannot retain the topmost layer and the copper paste (Fig. 4a). This issue is solved by applying the paste onto an already fused part of solid metal since here the adhesive forces are sufficient to prevent the paste from being dragged along with the dispenser (Fig. 4b).

When applying a new layer of metal powder for the LPBF process after fusing the Cu structure, at times there were issues with the recoating process a) when the laser had not exposed the entire contour of the applied paste or b) when spraying patterns of copper and other waste products accumulated in the powder bed (Fig. 4d). These are generated by the interaction of laser and paste, comparable to the spattering in the LPBF process [24]. Similar to the spatter formation in the LPBF process, the paste spattering might be caused as a result of the pushback pressure of the melting pool. In addition, a very clear smoke plume was observed, which produced dark spots on the powder bed. These spots were elongated and aligned parallel to the shielding gas flow. The resulting inhomogeneities are illustrated in Figure 5. The process inhomogeneities and the extremely dynamic process can be explained by insufficiently pre-dried structures. Since a material loss greater than the amount of solvent contained in the paste was observed during the drying step, it was previously assumed that the structures had dried out. However, it appears that organic additives were still present in the structures and lead to the observed dynamic processes and process inhomogeneities. The produced spatters in the powder bed and unexposed parts of the Cu structures then stuck to the recoater or were dragged along by it, leading to an inhomogeneous powder layer for the LPBF process. Finally, since powder application even after exposure and remelting of the deposited paste lead to this influence on the coater tool and the powder layer quality, powder application on an unexposed structure was not considered (Fig. 4c).

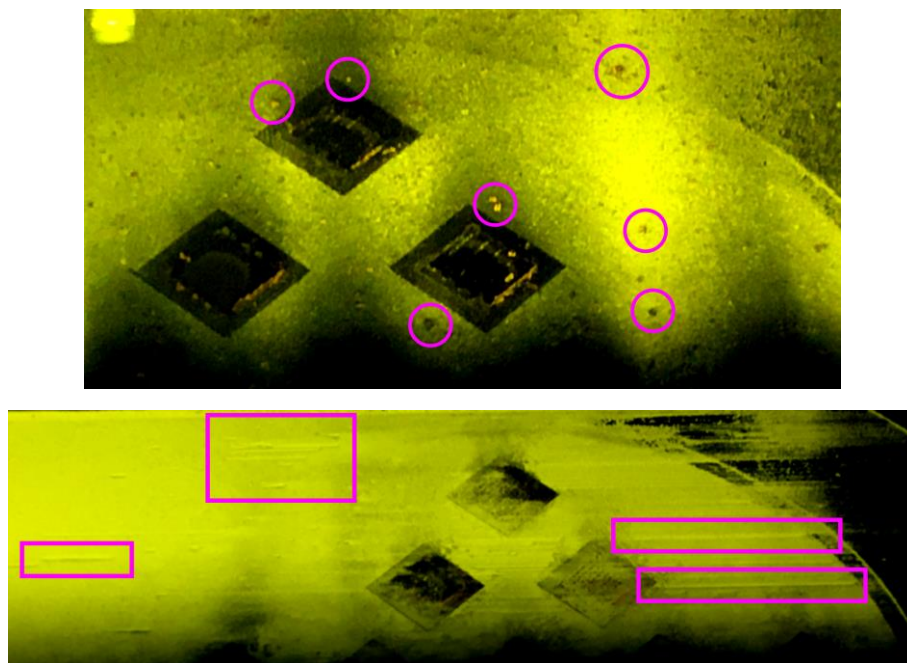


Figure 5: Illustration of the influence of the exposure process on the formation of inhomogeneities (top) and the impact on the coater process as a result of the formed inhomogeneities (bottom)

3.3. Drop-on-demand vs. continuous approach for materials application

To compare the film quality produced by either DoD and continuous deposition, test specimens were

produced that consisted of four copper dots in each corner of a cube surface and a meander-shaped surface in the center of the cube surface (Fig. 3). The cubes were produced by LPBF out of 316L stainless steel. The comparison between the points applied via the DoD approach and the area of copper paste applied via the continuous approach was performed by energy-dispersive X-ray spectroscopy (EDX) analysis of the structures under consideration. A distinction was made between structures which consisted of ten layers of Cu paste (referred to as “high amount of Cu”) and others which consisted of only three layers (“low amount of Cu”). The EDX measurements served to determine whether it is possible in principle to influence the chemical composition via the additional aggregates and if the detected copper contents correlate positively with the amount of material applied.

In fact, such a behavior can be traced in the EDX measurements (Fig. 6). The values for the Cu and Fe detected show an inverse behavior, showing that either the Cu structure or the underlying steel is detected. This is especially obvious for the DoD samples which show a very high fluctuation in Cu content, which speaks of a discontinuous Cu layer with many holes. In contrast, the samples produced by a continuous deposition show a much more homogeneous distribution, however still with some spots where Fe was detected, meaning even here some holes in the film are present. In spite of the higher homogeneity in the measured values, for the low amount of copper paste applied only small amounts of copper were detected (< 20 wt%). This can be explained by a homogeneous distribution of small Cu particles below the step size of the EDX measurement of ca. 100 μm , while for the DoD samples the holes in the layer must be close to 100 μm in size. In contrast, the samples with a high Cu amount indeed show higher Cu values between 75-90 wt% in the EDX analysis. The remaining weight is made up mostly of carbon, which probably comes from impurities produced from the organic molecules in the Cu paste. In summary, the continuous approach is more promising, but still needs improvement to achieve dense films made of up 100% copper.

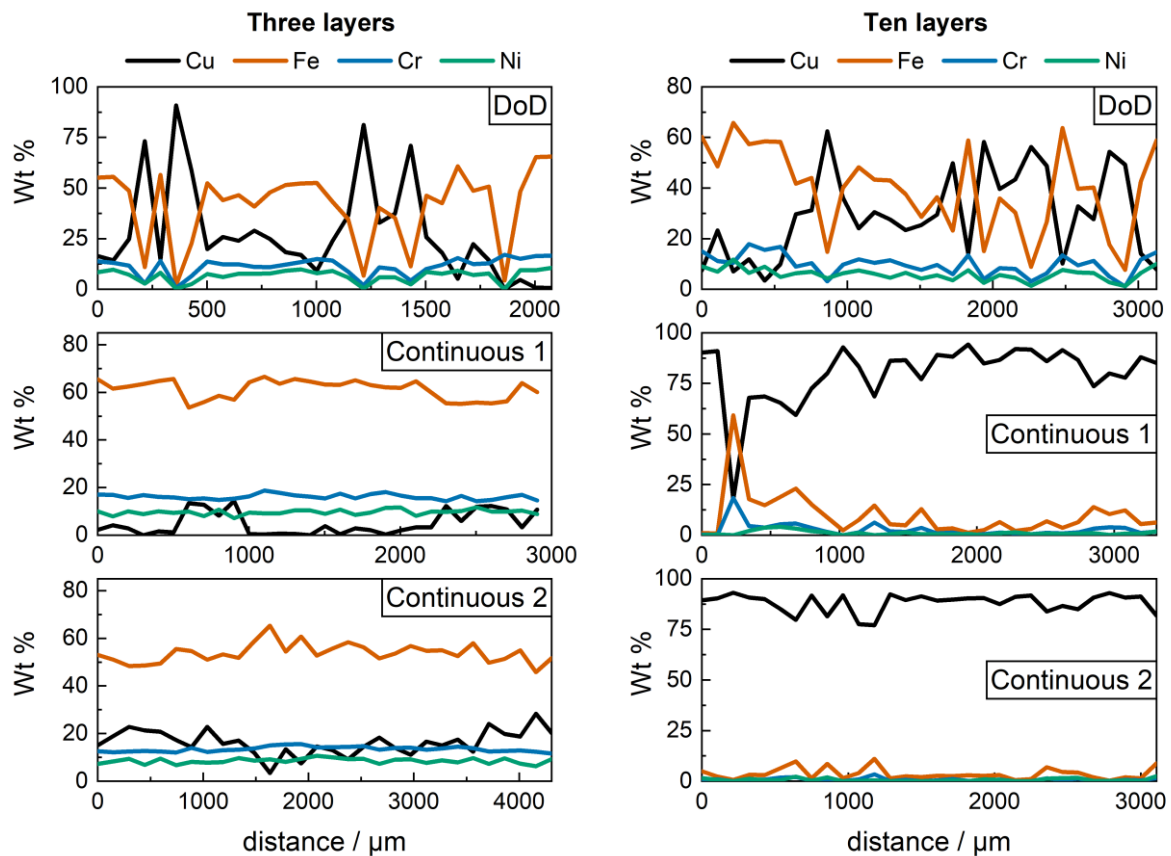


Figure 6: EDX measurement - comparison of DoD approach and continuous approach of material application for low copper amounts (left) versus high copper amounts (right)

4. Conclusion & Outlook

Combining the LPBF process with a dispensing system is a promising approach to build up three-dimensional multi-material AM parts. In this paper, a machine concept for the integration of LPBF with two deposition technologies was presented and the relevant process parameters regarding the dispensing system were investigated. The feasibility to use this approach to locally adapt the chemical composition was shown by successful drop-on-demand and continuous material deposition of a copper paste on stainless steel substrates. The travel speed of the dispenser as well as the exposure time during the subsequent drying and fusion are the most important parameters regarding the quality of the resulting structures. With an increasing speed for continuous material, the characteristics of the track- width and height decreases. For the DoD approach the diameter as well as the spot height increases with a higher dwell time.

The deposition was followed by drying and fusion which were carried out by the LPBF laser to reduce the number used components as much as possible. However, in the scope of this work the parameters for the laser exposure could not be optimized in a way that produces dense and defect-free, 100% pure Cu structures. The main impediment was an explosive evaporation of the organic molecules contained in the paste caused by the high laser power, which led to damage to the film. In addition, in

many cases the drying step was not complete. To avoid this, a reduction in the laser power and lower process speeds will have to be achieved or an alternative way of drying the paste employed, such as an IR lamp. These studies will be accompanied by an improved detection of remaining organics in the dried film by chemical analysis.

In addition, variations in the order of material deposition and laser exposition were studied and the strict separation of LPBF and dispenser was identified as the most promising route. In the case of embedded structures, the drying and fusion of the deposited structures must be complete in order not to affect the following LPBF process. In this context, future studies will investigate the interface between the LPBF substrate and the Cu structure, especially the adhesion between the two.

Future work in this area will also include the aerosol jet printing unit of the integrated setup that will allow adding material with a much finer spatial resolution and lower film thickness as well as open up a wide range of possible materials.

5. Literature

- [1] Bandyopadhyay, A.; Heer, B.: Additive manufacturing of multi-material structures. In: *Materials Science and Engineering: R: Reports* 129, 2018, S. 1–16. DOI: 10.1016/j.mser.2018.04.001.
- [2] Gebhardt, Andreas: Additive Fertigungsverfahren. Additive Manufacturing und 3D-Drucken für Prototyping - Tooling - Produktion. [5., neu bearbeitete und erweiterte Auflage: Hanser. München, 2016.
- [3] Senthilkumar, V.; Velmurugan, C.; Balasubramanian, K. R.; Kumaran, M.: Additive Manufacturing of Multi-Material and Composite Parts. In: K. R. Balasubramanian und V. Senthilkumar (Hg.): *Additive Manufacturing Applications for Metals and Composites: Engineering Science Reference*. Hershey, PA, 2020, S. 127–146.
- [4] DebRoy, T.; Wei, H. L.; Zuback, J. S.; Mukherjee, T.; Elmer, J. W.; Milewski, J. O. et al.: Additive manufacturing of metallic components – Process, structure and properties. In: *Progress in Materials Science* 92, 2018, S. 112–224. DOI: 10.1016/j.pmatsci.2017.10.001.
- [5] Hopkinson, N.; Hague, R. J. M.; Dickens, P. M.: *Rapid manufacturing. An industrial revolution for the digital age*: John Wiley. Chichester England, 2006.
- [6] Cui, Zheng (Hg.), 2016: *Printed Electronics: Materials, Technologies and Applications*. Singapore: John Wiley & Sons Singapore Pte. Ltd.
- [7] Chen, Z.: Inorganic Printable Electronic Materials. In: Zheng Cui (Hg.): *Printed Electronics: Materials, Technologies and Applications*: John Wiley & Sons Singapore Pte. Ltd. Singapore, 2016, S. 54–105.
- [8] Agarwala, S.; Goh, G. L.; Dinh Le, T.-S.; An, J.; Peh, Z. K.; Yeong, W. Y.; Kim, Y.-J.: Wearable Bandage-Based Strain Sensor for Home Healthcare: Combining 3D Aerosol Jet Printing and Laser Sintering. In: *ACS sensors* 4, 2019 (1), S. 218–226. DOI: 10.1021/acssensors.8b01293.
- [9] Neirinck, B.; Li, X.; Hick, M.: Powder Deposition Systems Used in Powder Bed-Based Multimetal Additive Manufacturing. In: *Acc. Mater. Res.*, 2021. DOI: 10.1021/accountsmr.1c00030.

- [10] DebRoy, T.; Wei, H. L.; Zuback, J. S.; Mukherjee, T.; Elmer, J. W.; Milewski, J. O. et al.: Additive manufacturing of metallic components – Process, structure and properties. In: *Progress in Materials Science* 92, 2018, S. 112–224. DOI: 10.1016/j.pmatsci.2017.10.001.
- [11] Wei, C.; Li, L.; Zhang, X.; Chueh, Y.-H.: 3D printing of multiple metallic materials via modified selective laser melting. In: *CIRP Annals* 67, 2018 (1), S. 245–248. DOI: 10.1016/j.cirp.2018.04.096.
- [12] Novacentrix: Safety Data Sheet. Metalon CP-009 Copper Paste for Laser and Photonic Sintering, 2019. Online verfügbar unter <https://www.novacentrix.com/datasheet/Metalon-CP-009-SDS.pdf>.
- [13] Tan, H. W.; An, J.; Chua, C. K.; Tran, T.: Metallic Nanoparticle Inks for 3D Printing of Electronics. In: *Adv. Electron. Mater.* 5, 2019 (5), S. 1800831. DOI: 10.1002/aelm.201800831.
- [14] ViscoTec Pumpen- u. Dosiertechnik GmbH: Betriebs- und Wartungsanleitung. eco-PEN330, 2020. Online verfügbar unter https://www.dosieren.de/media/pdf/c7/06/6b/eco-PEN330_MAN_de.pdf.
- [15] ViscoTec Pumpen- u. Dosiertechnik GmbH: Betriebs- und Wartungsanleitung. eco-Control EC200-B, 2019. Online verfügbar unter https://www.dosieren.de/media/pdf/77/3e/38/eco-EC200-B_MAN_DE.pdf.
- [16] Tian, X.; Jin, J.; Yuan, S.; Chua, C. K.; Tor, S. B.; Zhou, K.: Emerging 3D-Printed Electrochemical Energy Storage Devices: A Critical Review. In: *Adv. Energy Mater.* 7, 2017 (17), S. 1700127. DOI: 10.1002/aenm.201700127.
- [17] Härtel, A.; Scheithauer, U.; Schwarzer, E.; Weingarten, S.; Slawik, T.; Richter, H.-J.; Moritz, T.: Additive Herstellung mehrkomponentiger metallischer und keramischer Bauteile mittels Thermoplastischen 3D-Druckes (T3DP). In: *Keram. Z.* 68, 2016 (1), S. 43–47. DOI: 10.1007/BF03400410.
- [18] Rafiee, M.; Farahani, R. D.; Therriault, D.: Multi-Material 3D and 4D Printing: A Survey. In: *Advanced science (Weinheim, Baden-Wuerttemberg, Germany)* 7, 2020 (12), S. 1902307. DOI: 10.1002/advs.201902307.
- [19] Kumar, Sanjay: Additive Manufacturing Processes: Springer International Publishing. Cham, 2020.
- [20] Kwon, K.-S.; Rahman, M. K.; Phung, T. H.; Hoath, S.; Jeong, S.; Kim, J. S.: Review of digital printing technologies for electronic materials. In: *Flex. Print. Electron.*, 2020. DOI: 10.1088/2058-8585/abc8ca.
- [21] ASM International: ASM handbook, Volume 24. Additive Manufacturing Processes: ASM Internat. Materials Park, Ohio, 2020.
- [22] Grden, M.; Skkietitbutra, J.; Vollertsen, F.; Johnigk, C.; Emonts, M.; Brecher, C.; Eckert, M.: Prozessauslegung beim Laserstrahlunterstützten Stanzen. In: *LTI* 7, 2010 (6), S. 36–41. DOI: 10.1002/latj.201090091.
- [23] Albery, W. J.; Greenwood, A. R.; Kibble, R. F.: Diffusion Coefficients of Carboxylic Acids. In: *Transactions of the Faraday Society* 63, 1967, S. 360–368. DOI: 10.1039/TF9676300360.
- [24] Yin, J.; Wang, D.; Yang, L.; Wei, H.; Dong, P.; Ke, L. et al.: Correlation between forming quality

and spatter dynamics in laser powder bed fusion. In: *Additive Manufacturing* 31, 2020, S. 100958.
DOI: 10.1016/j.addma.2019.100958.

Contact

Jonas Boseila

RWTH Aachen University, Digital Additive Production (DAP)
Campus-Boulevard 73
52074 Aachen, Germany
Email: jonas.boseila@dap.rwth-aachen.de
WEB: www.dap-aachen.de

Max Rommerskirchen

RWTH Aachen University, Digital Additive Production (DAP)
Campus-Boulevard 73
52074 Aachen, Germany
Email: max.rommerskirchen@dap.rwth-aachen.de

Sebastian Bold

RWTH Aachen University, Digital Additive Production (DAP)
Campus-Boulevard 30
52074 Aachen, Germany
Email: sebastian.bold@dap.rwth-aachen.de

Johannes Henrich Schleifenbaum

RWTH Aachen University, Digital Additive Production (DAP)
Campus-Boulevard 73
52074 Aachen, Germany
Email: johannes.henrich.schleifenbaum@dap.rwth-aachen.de